Affine transformations for purely anisotropic cloaking in flexural elastic thin plates

Léo Pradier[1], Grégoire Pizon[2], Valentin Rapine[3], Baptiste Chomette[1], Morvan Ouisse[2], Arnaud Hubert[4], and Manuel Collet*,[1]

[1]Ecole Centrale de Lyon, CNRS, ENTPE, LTDS, UMR5513, 69130 Ecully, France
[2]Université Marie et Louis Pasteur, CNRS, Institut FEMTO-ST, 25000 Besançon, France
[3]Université Savoie Mont-Blanc, SYMME, Annecy, 74000, France
[4]Université de Technologie de Compiègne, Alliance Sorbonne Université, Laboratoire Roberval, Centre de recherche de Royallieu, CS 60319, 60203 Compiègne, cedex, France

Abstract

Cloaking for bending waves propagating in thin elastic plates is known to present numerous obstacles to its experimental realization, particularly due to the complexity of the effective medium obtained by coordinate transformation. Here we demonstrate the possibility of cloaking in a unidirectional manner using affine transformations. This class of transformations maps the Kirchhoff-Love plate equation to its anisotropic extension. Unlike most publications in the literature, the resulting cloak is easily manufacturable using composite materials. In addition to numerical demonstrations of the unidirectional cloaking phenomenon, we present here a design method of an effective cloaking device, as well as the experimental validation of the manufactured cloak.

1 Introduction

Cloaking consists of designing an area of space (the cloak) in such a way that the trajectory of waves entering it is modified. By appropriately determining the effective material properties of the cloak, the wave can be deflected so that it no longer interacts with a cloaked area. The cloak's properties must verify

*Corresponding author: manuel.collet@ec-lyon.fr

impedance matching condition with the host medium at its common boundary and a wave traveling through the cloak must retains its phase. Then, the wave field in the host medium remains the same as if there were no cloak and cloaked area (initial homogeneous media). The first publications on cloaking for electromagnetic radiation are based on a transformation of space coordinates [1,2]. This involves mapping the coordinates in such a way as to open up a spatial void: the cloaked area. This new coordinate system is used to derive the cloaking equation, *i.e.* the propagation equation (in the latter, Maxwell's equations) with respect to these new coordinates. It is then shown that the cloaking equation can be reproduced in physical space by using an anisotropic and heterogeneous effective medium, which has been approximated by metamaterials [3, 4]. This method appears to be conclusive for other hyperbolic propagation equations [5–10]. For instance, transformation acoustics enables the realization of acoustic mirages through the use of anisotropic media [11] and omnidirectional cloaking using more general anisotropic and heterogeneous media [12–14]. In the case of 3D elasticity, governed by Navier equation, it is known that the latter is generally not form-invariant under coordinate transformation. This means that the cloaking equation cannot be reproduced using an anisotropic and heterogeneous medium. Instead, Navier equation is mapped to the Willis equation which includes anisotropic density [15] or using Cosserat elasticity, an equation with isotropic density but without minor symmetry of the elasticity tensor [16,17]. This encompasses microstructured materials that has been proved to be effective for in-plane elastic cloaking [18,19]. Simultaneously, cloaking for flexural guided waves that propagate in thin plates has been studied. Flexural waves result from the coupling of compressional and shear waves which leads to a dispersive behavior. A_0 flexural Lamb mode can be modeled in the low frequency regime using the fourth-order scalar-valued Kirchhoff-Love (KL) equation assuming a small thickness to wavelength ratio, $h/\lambda < 0.1$. Outside this range of validity, others models are required. Extensive studies [20–24] have investigated the KL cloaking problem and pointed out that KL equation is not form-invariant for radial push-out transformation. Contrary to acoustic cloaking where such transformations are used, discrepancies between the cloaking equation and the anisotropic heteregeneous KL model appear. The conclusion is that, there is no anisotropic and heterogeneous plate satisfying the transformed equation requirements. Form invariance of the thin-plate equation typically arises from the Kirchhoff-Love assumptions, which neglect shear deformations and out-of-plane stresses. The few experimental studies often neglect these discrepancies, leading to cloaking effectiveness limited to narrow frequency bands. The experiments presented in [25] were conducted between 200 and 450 Hz, and those in [26] appear to be conclusive below 270 Hz. A new framework emerged in 2014 from the work of Colquitt *et al.* [27] and Brun *et al.* [28]. It shows that the KL equation is mapped to von Kármán's anisotropic and heterogeneous plate equation [29,30] which includes space-dependent static pre-stress terms that match these additional terms in the transformed equation. However some authors have shown [24,31] that the host KL plate equation is not recovered when the transformation is set to identity. Another drawback is the not

positive-definite stiffness tensor of rank 1 used, associating null moments with non-null deformations (non-injective map). This leads to a material which is not physically feasible. More recently, Pomot *et al.* [31] correctly stated that KL equation remains invariant under affine coordinate transformation (the Hessian matrix of the tranformation is zero). Thus, satisfying cloaking equation is possible using purely anisotropic stiffness tensor in KL equation. Unfortunately, the numerical results they bring show that a significant portion of the incident wave is backscattered. It would appear that the translation of the plane stress stiffness tensor into the 3D elasticity tensor is incorrect. This nevertheless opened the way to the design of waveshifters [32] which has been use for cloaking application by Tang *et al.* [33, 34]. In the latter, authors show how to imitate cloaking behavior by guiding plane bending waves around a rhombus-shaped hole using four waveshifters rigidly connected and impedance-matched to the host isotropic plate. These anisotropic waveshifters successfully reconstruct the incident wavefront while minimizing scattering from the hole. It is nevertheless noted by authors that a phase delay between incident and transmitted waves appears, both numerically and experimentally. In accordance with the rules of perfect cloaking introduced in [35], phase conservation is a requirement, meaning that the methodology presented by Tang *et al.* [33] is an approximation of actual unidirectional cloaking.

In this paper, we will firstly show that the stiffness tensor used in their work is not compatible with anisotropic KL plate theory. Indeed, their model is based on classic acoustic cloaking theory and does not take into account the full complexity of bending waves since the latter are of a dispersive nature, unlike acoustic waves. Secondly, in agreement with the initial observations of Pomot *et al.* [31], we demonstrate the equivalence between the mapped form-invariant KL equation and the anisotropic KL equation. This allows us to determine the plate stiffness tensor satisfying unidirectional cloaking. It is important to note, however, that the proposed methodology is limited by the range of validity of the KL theory. All results presented here are given for the associated frequency range. More complex theories, such as Reissner-Mindlin or Rayleigh-Lamb models, could be used to generalize these results to high frequencies. However, the complexity of these models likely poses additional theoretical challenges and has therefore been little studied in the literature [36]. The KL theory remains relevant, however, in many low-frequency engineering applications. It is then shown that the obtained stiffness tensors correspond to those of anisotropic composite materials. Thirdly, numerical simulations are conducted to support our theoretical developments. We present the temporal evolution of a broadband burst in the time domain and develop a cloaking quality quantification indicator in the frequency domain. An analysis of the dispersion of the anisotropic material designed is performed in the fourth part, revealing interesting results concerning propagation of bending waves in cloaking layers. Fifthly, we present a method for designing an effective, manufacturable cloaking device based on optimization methods. The resulting design is manufactured and the experimental validation associated with it, is addressed in the sixth part.

2 The unidirectional cloaking problem

2.1 Anisotropic Kirchhoff-Love plate theory

We start by deriving the general governing PDE describing the out-of-plane displacement of a plate under Kirchhoff-Love hypotheses,

$$\nabla \cdot \nabla \cdot \boldsymbol{M} - \rho h \frac{\partial^2 w}{\partial t^2} = 0. \tag{1}$$

The solution $w(X_1, X_2, t) \in \mathbb{R}$ is the out-of-plane displacement in Cartesian coordinates, ρ and h are respectively mass density and plate's thickness. X_1 and X_2 are material coordinates in the midplane of the plate. $\boldsymbol{M}$ is the symmetric bending moment tensor,

$$\boldsymbol{M} = \begin{pmatrix} M_{11} & M_{12} \\ M_{12} & M_{22} \end{pmatrix}. \tag{2}$$

Its components are related to the displacement w through the constitutive law using Voigt notation,

$$\begin{pmatrix} M_{11} \\ M_{22} \\ M_{12} \end{pmatrix} = \boldsymbol{D}\boldsymbol{\kappa} = \begin{pmatrix} D_{11} & D_{12} & D_{16} \\ D_{12} & D_{22} & D_{26} \\ D_{16} & D_{26} & D_{66} \end{pmatrix} \begin{pmatrix} -\frac{\partial^2 w}{\partial X_1^2} \\ -\frac{\partial^2 w}{\partial X_2^2} \\ -2\frac{\partial^2 w}{\partial X_1 \partial X_2} \end{pmatrix}. \tag{3}$$

$\boldsymbol{D}$ and $\boldsymbol{\kappa}$ are the stiffness tensor and Voigt notated curvature tensor, respectively. One can show that $\boldsymbol{D}$ is related to $\bar{\boldsymbol{C}}$, the plane stress reduced elasticity tensor by the relation [30]:

$$\boldsymbol{D} = \frac{h^3}{12}\bar{\boldsymbol{C}}. \tag{4}$$

$\bar{\boldsymbol{C}}$ is obtained by imposing the components of the Cauchy stress tensor $\sigma_{i3} = 0$, with $i = \{1, 2, 3\}$. Using (2) and (3) in (1) and developing the two divergence operators, we obtain the general fourth-order anisotropic homogeneous plate equation:

$$\begin{aligned} D_{11}\frac{\partial^4 w}{\partial X_1^4} + 4D_{16}\frac{\partial^4 w}{\partial X_1^3 \partial X_2} + 2\left(D_{12} + 2D_{66}\right)\frac{\partial^4 w}{\partial X_1^2 \partial X_2^2} \\ + 4D_{26}\frac{\partial^4 w}{\partial X_1 \partial X_2^3} + D_{22}\frac{\partial^4 w}{\partial X_2^4} + \rho h \frac{\partial^2 w}{\partial t^2} = 0. \end{aligned} \tag{5}$$

2.2 Critical review of Tang's work

Here we briefly summarize the methodology presented by Tang *et al.* [32–34], emphasizing its limitations. They first introduce a spatial transformation of the form:

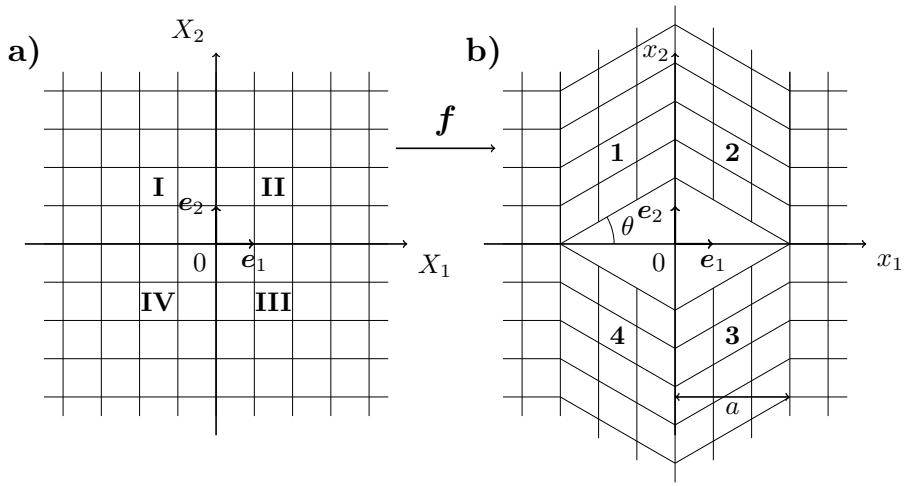

Figure 1: **a)**: Cartesian plane divided into four quadrants **I**, **II**, **III** and **IV**. **b)**: Cartesian plane piecewisely deformed by the transformation $\boldsymbol{f}$. It acts on $X_1 < a$ for quadrants **II** and **III**, and on $X_1 > -a$ for quadrants **I** and **IV**. It results the four transformed domains **1**, **2**, **3**, **4**. Note that the transformed (convected) coordinate lines do not represent the coordinate lines associated with coordinates $\boldsymbol{x}$, but rather the image of the coordinate lines associated with material coordinates $\boldsymbol{X}$ by the transformation $\boldsymbol{f}$.

$$\boldsymbol{x} = \boldsymbol{f}(\boldsymbol{X}) = \begin{cases} X_1 \\ X_1 \tan(\theta) + X_2 \end{cases}, \tag{6}$$

that maps the Cartesian space (described by the material coordinates $\boldsymbol{X} = (X_1, X_2)^t$) to a holed space (described by the material coordinates $\boldsymbol{x} = (x_1, x_2)^t$). θ is the opening angle of the hole. Applying transformations of this form on each four quadrant of the plane opens up a rhomboid-shaped spatial void representing the cloaked area. Transformation applied to Cartesian grid is shown in figure 1. Then, based on literature of cloaking for dispersionless acoustic waves in non-shearable fluids, they state that the anisotropic stiffness tensor satisfying cloaking can be obtained by applying twice Norris' lemma 2.1 [12]:

$$\boldsymbol{D} = D\,\boldsymbol{F}\boldsymbol{F}^t\boldsymbol{F}\boldsymbol{F}^t J^{-2}. \tag{7}$$

Where $\boldsymbol{F} = \nabla \boldsymbol{f}$, (so $F_{ij} = \frac{\partial x_i}{\partial X_j}$) is the transformation gradient. D is the stiffness of the homogeneous isotropic host plate and $J = \det(\boldsymbol{F})$, the jacobian. The proposed stiffness is a 2×2 matrix, which does not correspond to the 3×3 KL stiffness matrix defined in section 2.1. It is not clearly specified which linear map this matrix is characteristic of, but in any case considering such a matrix leads to eliminate one of the moments and one of the curvatures while decoupling the remaining moments from this curvature. None of these cases is compatible with the theory of plate's bending. In what next, they state that (7) can be approximated by an effective obliquely-oriented bilayered laminate, following the design methodology from [37]. All cloaking results presented both numerically and experimentally are based on this substructured plate composed of alternating layers of stiffness D_a and D_b. It is not explicitly explained how to determine the properties of the laminate starting from (7), but it is clear that such a structure could be homogenized using the anisotropic KL plate theory with an actual stiffness tensor of the form of (3). It is important to note that considering the homogenization of the laminate will not lead to the formulation of unidirectional cloaking due to the obtained phase shift underlining limitations of this approach. This cloaking approximation is nevertheless capable of effectively route a plane wave around an hole while minimizing scattering. As pointed out by authors in [32], the quality of cloaking deteriorates as θ increases. This parameter defines the required degree of anisotropy, and the stiffness terms that were previously neglected in (7) can no longer be ignored. The work presented here is an extension of this approach in which all the stiffness coefficients are derived.

2.3 Derivation of the cloaking equation

Now let us consider the mapping of the homogeneous isotropic KL equation to the deformed configuration. We start here with the homogeneous isotropic KL equation, derived from (5) using the following isotropic stiffness tensor,

$$\boldsymbol{D}_{\text{iso}} = \begin{pmatrix} D & \nu D & 0 \\ \nu D & D & 0 \\ 0 & 0 & \frac{1}{2}(D-\nu D) \end{pmatrix} \quad \text{[N.m]}. \tag{8}$$

Here, $D = Eh^3/(12(1-\nu^2))$ is the bending stiffness coefficient of an homogeneous isotropic plate. E is the Young's modulus and ν the Poisson's ratio. We then obtain the following equation of motion,

$$D\Delta^2 w + \rho h \frac{\partial^2 w}{\partial t^2} = 0. \tag{9}$$

$\Delta^2 = \frac{\partial^4}{\partial X_1^4} + 2\frac{\partial^4}{\partial X_1^2 X_2^2} + \frac{\partial^4}{\partial X_2^4}$ is the bilaplacian operator in Cartesian coordinates. Using differential geometry, the Laplace-Beltrami operator in any coordinate system reads,

$$\Delta = \frac{1}{\sqrt{g}} \partial_i \left(\sqrt{g} g_{ij}^{-1} \partial_j \right), \tag{10}$$

where Einstein summation convention is applied. Taking the inverse transformation $\boldsymbol{X} = \boldsymbol{f}^{-1}(\boldsymbol{x})$, $\boldsymbol{g} = (\nabla \boldsymbol{f}^{-1})^t \nabla \boldsymbol{f}^{-1}$ is the metric tensor induced by $\boldsymbol{f}^{-1}$. Its gradient $\nabla \boldsymbol{f}^{-1}$ is written in index notation $(\nabla \boldsymbol{f}^{-1})_{ij} = \frac{\partial X_i}{\partial x_j}$. $g = |\boldsymbol{g}|$ is the determinant of $\boldsymbol{g}$. From (10), one can derive the mapped bilaplacian $\Delta^2 = \Delta\Delta$:

$$\Delta^2 = \frac{1}{\sqrt{g}} \partial_i \left(\sqrt{g} g_{ij}^{-1} \partial_j \left(\frac{1}{\sqrt{g}} \partial_k \left(\sqrt{g} g_{kl}^{-1} \partial_l \right) \right) \right). \tag{11}$$

For the sake of subsequent developments, derivatives of $\boldsymbol{g}^{-1}$ in (11), are written as follows:

$$\nabla \boldsymbol{g}^{-1} = (\nabla \boldsymbol{f}^{-1})^{-1} \boldsymbol{H} \boldsymbol{g}^{-1} + \boldsymbol{g}^{-1} \boldsymbol{H}^\dagger \nabla (\boldsymbol{f}^{-1})^{-t}. \tag{12}$$

$\boldsymbol{H} = \nabla\nabla \boldsymbol{f}^{-1}$ and $\boldsymbol{H}^\dagger = \nabla \left(\nabla \boldsymbol{f}^{-1} \right)^t$ are Hessian matrices that vanish if $\boldsymbol{f}^{-1}$ is affine. By fully developing (11) under this hypothesis, it comes,

$$\Delta^2 = \frac{1}{\sqrt{g}} g_{ij}^{-1} g_{kl}^{-1} \partial_{ijkl}. \tag{13}$$

For the four quadrants **I**, **II**, **III** and **IV**, the transformation $\boldsymbol{f}$ is,

$$(x_1, x_2)^t = \begin{cases} \boldsymbol{f}^{(1)}(X_1, X_2) = \big(X_1,\ \tan(\theta) X_1 + X_2 + a\tan(\theta)\big) & \text{for } X_1 \in [-a, 0],\ X_2 > 0, \\ \boldsymbol{f}^{(2)}(X_1, X_2) = \big(X_1,\ -\tan(\theta) X_1 + X_2 + a\tan(\theta)\big) & \text{for } X_1 \in [0, a],\ X_2 > 0, \\ \boldsymbol{f}^{(3)}(X_1, X_2) = \big(X_1,\ \tan(\theta) X_1 + X_2 - a\tan(\theta)\big) & \text{for } X_1 \in [0, a],\ X_2 < 0, \\ \boldsymbol{f}^{(4)}(X_1, X_2) = \big(X_1,\ -\tan(\theta) X_1 + X_2 - a\tan(\theta)\big) & \text{for } X_1 \in [-a, 0],\ X_2 < 0. \end{cases} \tag{14}$$

Taking for instance $\boldsymbol{f}^{(1)}$ the transformation associated with quadrant **I** we write the mapped bilaplacian (13) in the spatial coordinates $\boldsymbol{x}$. Using this in the isotropic homogeneous KL equation (9), we get the cloaking equation:

$$\begin{aligned} D\frac{\partial^4 w}{\partial x_1^4} + 4D\tan(\theta)\frac{\partial^4 w}{\partial x_1^3 \partial x_2} + D\left(2+6\tan(\theta)^2\right)\frac{\partial^4 w}{\partial x_1^2 \partial x_2^2} \\ + D\left(4\tan(\theta)+4\tan(\theta)^3\right)\frac{\partial^4 w}{\partial x_1 \partial x_2^3} \\ + D\left(1+2\tan(\theta)^2+\tan(\theta)^4\right)\frac{\partial^4 w}{\partial x_2^4} + \rho h\frac{\partial^2 w}{\partial t^2} = 0. \end{aligned} \quad (15)$$

We note that the cloaking equation (15) only depends on the fourth-order derivatives of w because of the form of (13). Comparison with the anisotropic KL plate equation (5) proves the form-invariance of KL equation (9) under this affine transformation.

2.4 Effective stiffness tensors

Equations (9) and (15) are essentially the same, they describe wave propagation in an homogeneous isotropic medium relatively to two different representations $\boldsymbol{X}$ and $\boldsymbol{x}$. Relatively to our point of view, the plane wave solution of (15) appears vertically sheared. We note that basis vectors $(\boldsymbol{e}_1, \boldsymbol{e}_2)$ associated with coordinates $\boldsymbol{X}$ and $\boldsymbol{x}$ are the same. Thus, thanks to the form-equivalence between (5) and (15), choosing the coefficients of (5) in such a way that they match those of (15) correspond to reproduce the shear effect in the $\boldsymbol{X}$ representation. This leads to a system of linear algebraic equations solved for D_{ij},

$$\begin{cases} D_{11} = D \\ 4D_{16} = 4D\tan(\theta) \\ 2(D_{12}+2D_{66}) = 2D + 6D\tan(\theta)^2 \\ 4D_{26} = 4D\tan(\theta) + 4D\tan(\theta)^3 \\ D_{22} = D + 2D\tan(\theta)^2 + D\tan(\theta)^4 \end{cases} . \quad (16)$$

D_{11}, D_{22}, D_{16}, and D_{26} are determined straightforwardly. The last equation relating D_{12} and D_{66} remains underdetermined. Taking into account that $\boldsymbol{D}^{(1)}$ (stiffness tensor of domain 1) must be equal to $\boldsymbol{D}_{\text{iso}}$ when $\theta = 0$ (so $\boldsymbol{f}$ becomes the identity transformation), one can identify two solutions for $\boldsymbol{D}^{(1)}$ by letting either $D_{12} = \nu D + \beta(\theta)$ or $D_{66} = 1/2(D - \nu D) + \beta(\theta)$. β is an arbitrary function satisfying $\beta(0) = 0$. We only consider the constraint on D_{12} in what follows. This gives the solution,

$$\boldsymbol{D}^{(1)} = \begin{cases} D_{11} = D \\ D_{12} = \nu D + \beta(\theta) \\ D_{16} = D\tan(\theta) \\ D_{22} = D + 2D\tan(\theta)^2 + D\tan(\theta)^4 \\ D_{26} = D\tan(\theta) + D\tan(\theta)^3 \\ D_{66} = \frac{1}{2}(D - \nu D + 3D\tan(\theta)^2 - \beta(\theta)) \end{cases} . \tag{17}$$

We note that $\boldsymbol{D}_{\text{iso}}$ is recovered at $\theta = 0$, for all D_{ij}. Applying the same procedure for the remaining transformations $\boldsymbol{f}^{(2)}$, $\boldsymbol{f}^{(3)}$ and $\boldsymbol{f}^{(4)}$, one can proves that $\boldsymbol{D}^{(3)} = \boldsymbol{D}^{(1)}$ and $\boldsymbol{D}^{(4)} = \boldsymbol{D}^{(2)}$. The expression of $\boldsymbol{D}^{(2)}$ is,

$$\boldsymbol{D}^{(2)} = \begin{cases} D_{11} = D \\ D_{12} = \nu D + \beta(\theta) \\ D_{16} = -D\tan(\theta) \\ D_{22} = D + 2D\tan(\theta)^2 + D\tan(\theta)^4 \\ D_{26} = -D\tan(\theta) - D\tan(\theta)^3 \\ D_{66} = \frac{1}{2}(D - \nu D + 3D\tan(\theta)^2 - \beta(\theta)) \end{cases} . \tag{18}$$

It seems interesting to study the symmetries of these tensors. Such tensors could, for example, represent those of an orthotropic material (three orthogonal planes of symmetry) whose principal directions of orthotropy are not $\boldsymbol{e}_1$ and $\boldsymbol{e}_2$. We are therefore looking for a presumed local basis $(\boldsymbol{e}_L, \boldsymbol{e}_T)$, resulting from an angular rotation α of basis vectors $\boldsymbol{e}_1$ and $\boldsymbol{e}_2$. This new basis is depicted in Figure 2.

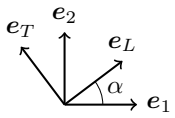

Figure 2: Local basis definition

The elasticity matrix $\bar{\boldsymbol{C}}^{(1)} = 12/h^3\boldsymbol{D}^{(1)}$ from (4), written in this local basis is [38],

$$\bar{\boldsymbol{C}}^{(1)'}(\alpha) = \boldsymbol{T}(\alpha)\bar{\boldsymbol{C}}^{(1)}\boldsymbol{R}\boldsymbol{T}^{-1}(\alpha)\boldsymbol{R}^{-1}. \tag{19}$$

$\boldsymbol{R} = \text{diag}(1, 1, 2)$ is the Reuter's matrix relating the strain tensor to engineering strain vector. $\boldsymbol{T}(\alpha)$ is the Voigt notated stress tensor's rotation matrix:

$$\boldsymbol{T}(\alpha) = \begin{pmatrix} \cos(\alpha)^2 & \sin(\alpha)^2 & 2\cos(\alpha)\sin(\alpha) \\ \sin(\alpha)^2 & \cos(\alpha)^2 & -2\cos(\alpha)\sin(\alpha) \\ -\cos(\alpha)\sin(\alpha) & \cos(\alpha)\sin(\alpha) & \cos(\alpha)^2 - \sin(\alpha)^2 \end{pmatrix}. \tag{20}$$

Table 1: Numerical parameters of the model

Name [unit]	Description	Value
L [m]	Host plate's size	0.5
h [m]	Plate's thickness	$3.36e-3$
a [m]	Cloaking layers' width	$8.3e-2$
θ [rad]	Shear angle (see Figure 1)	$\pi/6$
E [GPa]	Young's modulus	17.2
ν [1]	Poisson's ratio	0.3
ρ [kg/m^3]	Mass density	1756
$\beta(\theta)$ [1]	Stiffness tensor parameter	0
f_0 [Hz]	Burst center frequency	4500
ω_0 [rad/s]	Burst center angular frequency	$2\pi f_0$
D [N.m]	Host plate stiffness (see equation (8))	59.75
σ [1]	Gaussian standard deviation	$1e-4$
μ [1]	Gaussian expectation	$4.44e-4$

If there is an angle α that simultaneously satisfies $\bar{C}_{16}^{(1)'} = 0$ and $\bar{C}_{26}^{(1)'} = 0$, then $\bar{\boldsymbol{C}}^{(1)}$ is effectively orthotropic and α is the angle of a principal orthotropy direction. For $\alpha \in [-\pi/2, \pi/2]$, there are two solutions α_1 and α_2 giving orthogonal directions for $\boldsymbol{e}_L$. For each domain,

$$\begin{aligned}
\alpha_1^{(1,3)} &= \operatorname{atan}\left(\frac{1}{4}\left(-\sqrt{10+6\cos(2\theta)}\sec(\theta)+2\tan(\theta)\right)\right),\\
\alpha_2^{(1,3)} &= \operatorname{atan}\left(\frac{1}{4}\left(\sqrt{10+6\cos(2\theta)}\sec(\theta)+2\tan(\theta)\right)\right),\\
\alpha_1^{(2,4)} &= -\alpha_2^{(1,3)},\\
\alpha_2^{(2,4)} &= -\alpha_1^{(1,3)}.
\end{aligned} \tag{21}$$

with $\sec(\theta) = 1/\cos(\theta)$. We will show below that this feature greatly facilitates the design of the real structure. These relationships will be used for designing an orthotropic composite material in order to approximate effective stiffness given by equation (17).

3 Numerical results

Based on these initial theoretical developments, we now numerically solve the cloaking problem. The plate model available in COMSOL Multiphysics does not allow direct use of the reduced stress plane stress constitutive law. The results presented here are based on a mixed finite element formulation (implemented in the COMSOL Multiphysics' PDE module), often used for numerical solving of biharmonic problems [39–43]. This formulation consists of defining the bending moments M_{11}, M_{22}, and M_{12} as variables in addition to w. The

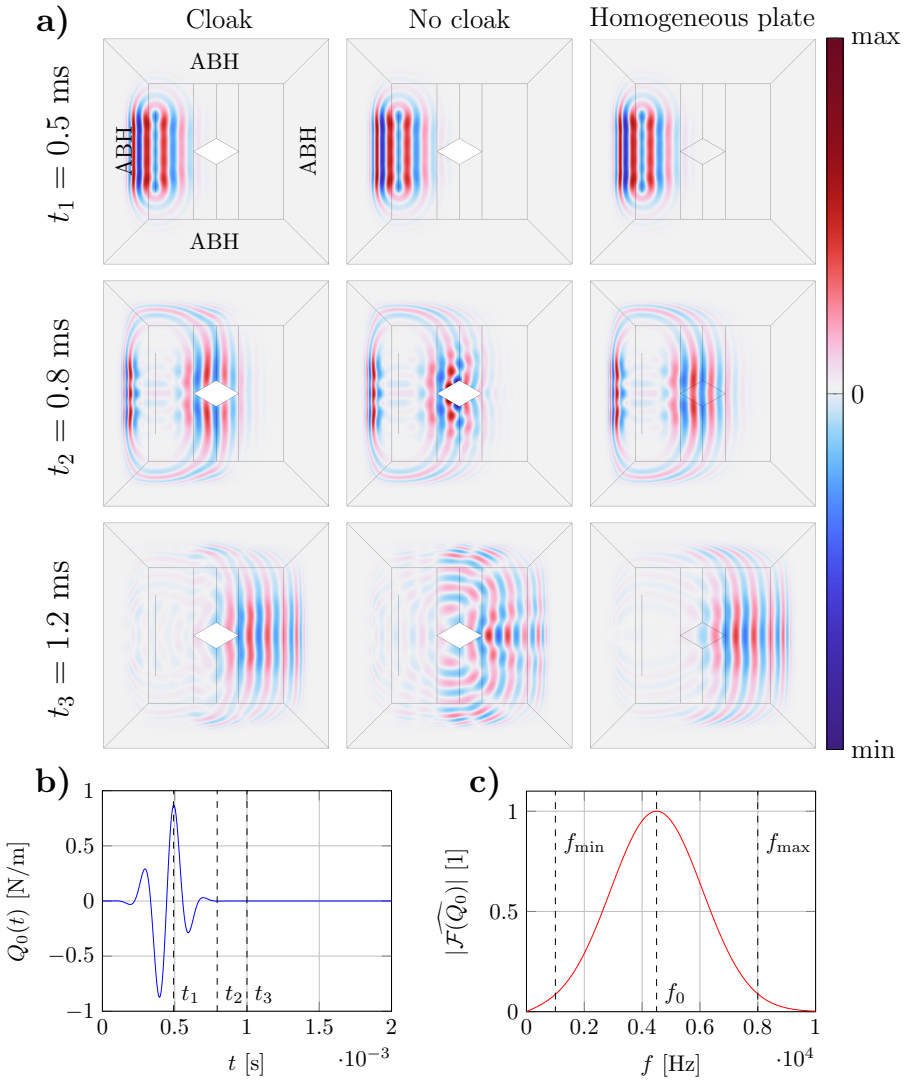

Figure 3: **a)** time domain simulation of a burst interacting with the cloaked hole (left panels), the uncloaked hole (middle panels), and the host plate alone (right panels). In all three cases, the displayed field is the out-of-plane velocity $v = \frac{\partial w}{\partial t}$. **b)** the considered burst and **c)**, its normalized spectrum.

second-order equations (1) and (3) are simultaneously solved instead of dealing with the fourth-order equation (5). This has the advantage of facilitating the specification of interface and boundary conditions, while reducing the order of test functions involved in the variational formulation. Numerical implementation is not further described here, but additional information are provided in the Supplemental Material.

Computed out-of-plane velocity $v = \frac{\partial w}{\partial t}$ in time domain using this mixed finite element formulation are shown in Figure 3. Part **a)** shows the temporal evolution of out-of-plane velocity field generated by a broadband gaussian burst, in three different configurations. The left panels show the wave propagating in the host plate and then in the cloaking layers surrounding a hole modeled by free edge boundary conditions. The middle panels show the wave propagating in the host plate with a hole. The right panels show the propagation of the wave in an homogeneous host plate without hole. Part **b)** illustrates the shear force $Q_0(t) = \sin(\omega_0 t)\exp\big(-(t-\mu)^2/(2\sigma^2)\big)$ applied to the excitation line, and part **c)** displays normalized modulus of its Fourier transform, $|\widehat{\mathcal{F}(Q_0)}| = |\mathcal{F}(Q_0)|/\max(|\mathcal{F}(Q_0)|)$. Gaussian parameters (given in Table 1) are chosen so that a broad frequency spectrum ranging from $f_{\min} = 1000$ to $f_{\max} = 8000$ Hz is covered. Absorbing layers imitating the Acoustic Black Hole (ABH) [44,45] effect are added to each of the edges of the host plate in order to eliminate reflections at boundaries. ABH involves defining a cubic profile with decreasing thickness toward the outside, slowing down the wave penetrating it. A cubically increasing outward viscous damping law (coefficienting $\frac{\partial w}{\partial t}$) is added to prevent the wave from being reflected back into the host plate. Numerical values of the parameters associated with this study are detailed in the Table 1. Numerical simulations clearly show the effectiveness of the proposed cloak. The cloak seems to successfully guiding the wave around the hole and reconstructing the plane wave without phase shift and scattering. We nevertheless note that a small portion of the energy is reflected backward (visible at $t = t_3$). This is due to the point of coordinates $(-a, 0)$, which belongs to the free edge of the hole but is not surrounded by cloaking layers. This point therefore acts as a scatterer. It is a drawback of the used transformation. Furthermore, the wave generated is not purely plane since the excitation line is finite. The extreme points of the line generate spherical waves penetrating the cloak at a non-zero angle of incidence and are then backscattered by the hole. We also note that residual reflections emanate from the ABH layers.

In the frequency domain, it is possible to define a quantification of scattering. As with time domain simulations, we numerically evaluate complex out-of-plane of the three velocity fields corresponding to the cloaked hole v_{cloak}, the hole without cloak v_{hole}, and the host plate without hole v_{host}. The scattering components in v_{cloak} and v_{hole} are the difference between these and the reference plane wave v_{host}. Out-of-plane velocity in frequency domain is $v = i\omega w$. The scattering field computation introduced is its normalized L^2 norm evaluate at a given frequency. For both v_{cloak} and v_{hole}, it reads,

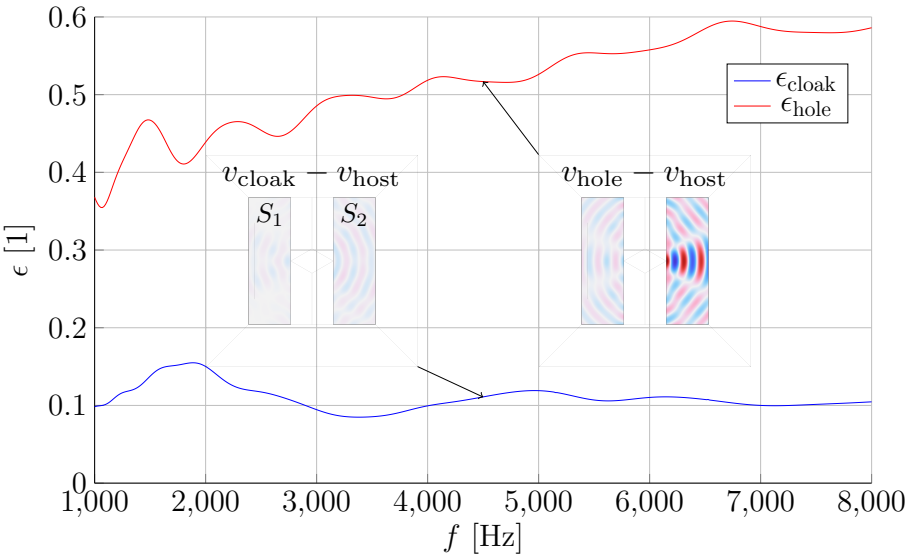

Figure 4: Scattering measurements ϵ_{cloak} and ϵ_{hole} plotted for $f \in [f_{\min}, f_{\max}] = [1000, 8000]$ Hz. The integrated scattering components $v_{\text{cloak}} - v_{\text{host}}$ and $v_{\text{hole}} - v_{\text{host}}$ are displayed for $f = 4500$ Hz.

$$\epsilon(v, v_{\text{host}}) = \frac{||v - v_{\text{host}}||_2}{||v_{\text{host}}||_2} = \left(\int_S |v - v_{\text{host}}|^2 \mathrm{d}S\right)^{1/2} \left(\int_S |v_{\text{host}}|^2 \mathrm{d}S\right)^{-1/2}. \quad (22)$$

The integration domain $S = S_1 \cup S_2$ used to compute this indicator is shown in Figure 4, as well as the scattering fields of v_{cloak} and v_{hole} at $f_0 = 4500$ Hz. In the same figure, we plot the scattering measurements ϵ_{cloak} and ϵ_{hole} for $f \in [1000, 8000]$ Hz. This clearly shows the frequency independence of the proposed cloak in this range. This frequency range was chosen so that the highest frequency $f_{\max}$ satisfies the Kirchhoff-Love validity criterion $h/\lambda < 0.1$. It should be noted that this scattering measurement is very sensitive to phase shift. Given the low values of ϵ_{cloak}, we conclude that there is no phase shift create by this cloak.

3.1 Dispersion analysis

Dispersion relations are obtained by assuming a plane wave solution $w = e^{i(\boldsymbol{k}\cdot\boldsymbol{X} - \omega t)}$ [46]. $\boldsymbol{k} = (k_1, k_2)^t$ is the wave vector, its norm $k = ||\boldsymbol{k}||$ is called wavenumber and its direction is the propagation direction. $\omega = 2\pi f$ is the angular frequency. Using the plane wave solution in anisotropic KL equation (5) leads to the following dispersion relation:

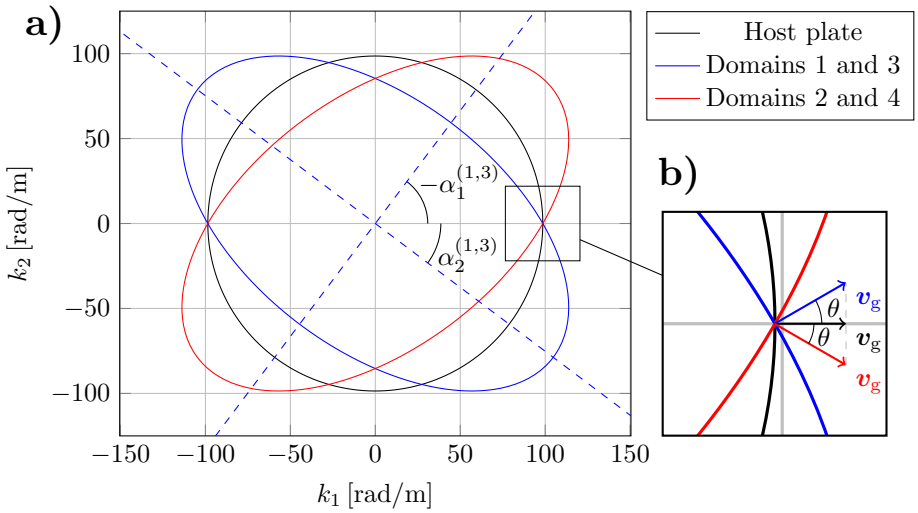

Figure 5: **a)** Isofrequency contour at $f = \omega/(2\pi) = 4500$ Hz of the dispersion relation (23). The black curve represents the isotropic host plate, while the blue and red curves represent domains 1,3 and 2,4 respectively. We note that principal axes (dashed blue lines for domains 1 and 3) of these contours are principal directions of orthotropy. **b)** Qualitative representation of group velocity vectors $\boldsymbol{v}_g$ for $k_2 = 0$. These vectors are always normal to the isofrequency contours.

$$\omega = \sqrt{\frac{D_{11}k_1^4 + 4D_{16}k_1^3k_2 + (2D_{12} + 4D_{66})k_1^2k_2^2 + 4D_{26}k_1k_2^3 + D_{22}k_2^4}{\rho h}}. \quad (23)$$

From the dispersion relation (23), we derive the bending wave's phase velocity $v_p = \omega/k$:

$$v_p = \sqrt{\frac{D_{11}k_1^4 + 4D_{16}k_1^3k_2 + (2D_{12} + 4D_{66})k_1^2k_2^2 + 4D_{26}k_1k_2^3 + D_{22}k_2^4}{\rho h(k_1^2 + k_2^2)}}. \quad (24)$$

Note that for a wave propagating in $\boldsymbol{e}_1$ direction, $k_2 = 0$. The phase velocity in this case reduced to $v_p = \sqrt{D_{11}k_1^2/(\rho h)}$. Since D_{11} is equal for both the host plate and the two different cloaking layers, phase velocity continuity is achieved. The directional derivative of ω with respect to the wave vector $\boldsymbol{k}$ is the group velocity $\boldsymbol{v}_g = \nabla_{\boldsymbol{k}}\omega$. Its norm is the wave packet velocity and its direction gives the one of energy flow. From equation (23),

$$\boldsymbol{v}_g = \begin{pmatrix} \frac{2D_{11}k_1^3+6D_{16}k_1^2k_2+(2D_{12}+4D_{66})k_1k_2^2+2D_{26}k_2^3}{\sqrt{\rho h(D_{11}k_1^4+4D_{16}k_1^3k_2+(2D_{12}+4D_{66})k_1^2k_2^2+4D_{26}k_1k_2^3+D_{22}k_2^4)}} \\ \frac{2D_{16}k_1^3+(2D_{12}+4D_{66})k_1^2k_2+6D_{26}k_1k_2^2+2D_{22}k_2^3}{\sqrt{\rho h(D_{11}k_1^4+4D_{16}k_1^3k_2+(2D_{12}+4D_{66})k_1^2k_2^2+4D_{26}k_1k_2^3+D_{22}k_2^4)}} \end{pmatrix}. \quad (25)$$

For $k_2 = 0$, this reduces to $\boldsymbol{v}_{\mathrm{g}} = \left(2D_{11}k_1/\sqrt{\rho h D_{11}},\, 2D_{16}k_1/\sqrt{\rho h D_{11}}\right)^t$. The $\boldsymbol{e}_1$ component of the group velocity vector is the same in the cloak as in the host plate. Due to anisotropy, the $\boldsymbol{e}_2$ component of the group velocity is not zero. The directions of propagation and energy flow are no longer collinear. This characteristic of anisotropic materials is known as wave skewing [47–49]. The skew angle is defined by $|\mathrm{atan}(v_{\mathrm{g}2}/v_{\mathrm{g}1}) - \phi|$, with ϕ the direction of propagation angle ($= 0$ in our case). One can show that this angle is, for $k_2 = 0$, equal to θ, the shear angle of the transformation (14). This shows that the coordinate transformation method developed in this article accurately defines a material that reproduces the desired shearing effect. By adopting the parametrization $(k_1, k_2) = (k\cos(\phi), k\sin(\phi))$ in (23), one can determine the stationary points $\frac{\partial k}{\partial \phi} = 0$ for a given ω. Values of ϕ associated with stationary points are the angles of principal axes of the isovalue curves obtained by imposing ω (isofrequency contour). These angles correspond to α, the angles associated with the principal directions of orthotropy. This confirms, from the point of view of dispersion, the orthotropic nature of the material. The results of the dispersion analysis are illustrated graphically in Figure 5. Isofrequency contour at $f_0 = 4.5$ kHz, for the cloaking layers and the isotropic host plate are presented as well as the group velocity vectors for $k_2 = 0$. Moreover, the dispersion analysis explains the absence of phase delay. Indeed, the normal incidence and the continuity of the phase velocity between the host plate and the cloaking layers ensure the conservation of the wave vector within the cloak. Direction and phase velocity are therefore the same as in the host plate. The flight time in the cloak is thus the same as in the host plate: no phase delay occurs. We have also seen that the component of the group velocity vector $v_{\mathrm{g}1}$ is conserved in the cloak, whereas the component $v_{\mathrm{g}2}$ is no longer zero as in the host plate. The group therefore follows a longer path in order to bypass the hole. It can be shown that the norm of the group velocity vector is such that this elongation is compensated for by the increase in group velocity. The group's flight time appears unchanged relative to the reference host plate: the group therefore also experiences no delay.

3.2 Incidence angle robustness

The robustness of the cloak at the angle of incidence is studied here. The shear force excitation is modified to include a spatial phase shift along the line:

$$Q_0 = e^{-ik(\omega)X_2\sin(\gamma)}e^{-i\omega t}. \tag{26}$$

γ is the angle of incidence of excited plane wave. The variation of ϵ criteria as a function of the latter is shown in the figure 6 for γ ranging from 0 (normal incidence) to 0.4 rad (approximately 23°). For these frequencies, the cloak always minimizes scattering compared to the bare hole according to ϵ criteria.

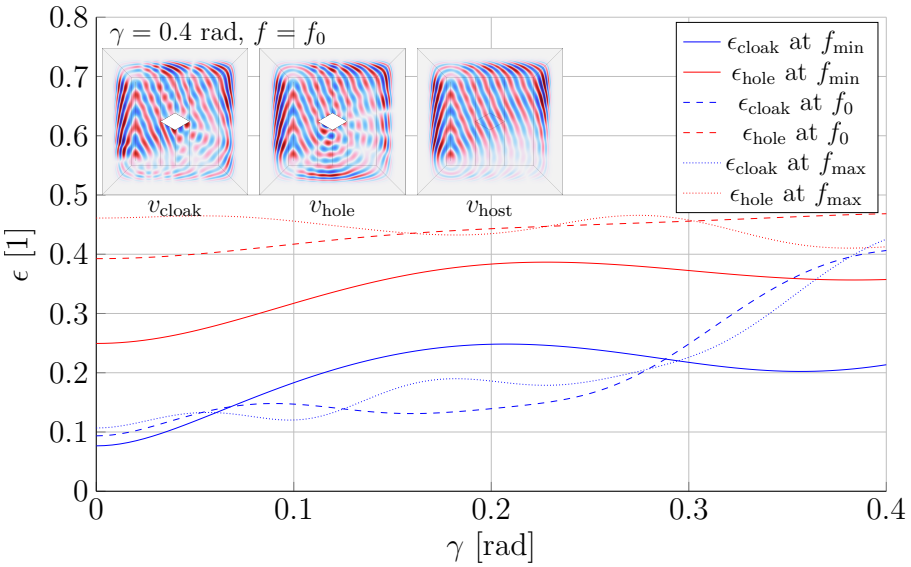

Figure 6: ϵ criteria as a function of γ, the angle of incidence for f_{min}, f_0, and f_{max}.

4 Design methodology of an effective cloaking device

The main difficulty in designing a manufacturable cloaking device stems from the fact that it is not straightforward to determine a real material (governed by 3D Hooke's law) starting from our reduced KL modeling in plane stress state. This section therefore deals with the inverse problem of determining a real material that best approximates the stiffness tensors $\boldsymbol{D}$ obtained in Section 2.4. This method is based on classical laminate theory [50] under the assumption of symmetry with respect to the midplane $X_3 = 0$. Their governing equation corresponds to the general equation (5) of an homogeneous anisotropic plate. The ability of such structures to influence the propagation of elastic waves is well known [47–49], enabling applications such as the focusing of flexural waves [51–53].

4.1 Stiffness tensor formulation from constitutive law of composite materials

We start here from the 3D Voigt notated Hooke law,

$$\boldsymbol{\sigma} = \boldsymbol{C}\boldsymbol{\varepsilon}. \tag{27}$$

$\boldsymbol{\sigma}$ and $\boldsymbol{\varepsilon}$ are 6×1 stress and strain vectors, respectively, and $\boldsymbol{C}$ is the 6×6

symmetric elasticity matrix. Let us assume a transversely isotropic material with an axis of symmetry included in the (X_1, X_2) plane. In this case, C_{14}, C_{15}, C_{24}, C_{25}, C_{34}, C_{35}, C_{46}, and C_{56} are zero. This typically models an unidirectional (UD) layer of fibers oriented in the direction of the axis of symmetry and impregnated with resin. Given the stated transverse isotropy and using what we introduced in Section 2.4, the angle α_f formed by the direction $\boldsymbol{e}_1$ and the direction of fibers allows us to define the local orthotropy basis $(\boldsymbol{e}_L, \boldsymbol{e}_T)$. $\boldsymbol{e}_L$ is pointing in the direction of fibers (see Figure 7). Inversing (19), we express $\bar{\boldsymbol{C}}$ with respect to $\bar{\boldsymbol{C}}'$, since material properties of UD layers are given in that local basis. Thus for a given orientated composite layer:

$$\bar{\boldsymbol{C}}(\alpha_\mathrm{f}) = \boldsymbol{T}^{-1}(\alpha_\mathrm{f})\bar{\boldsymbol{C}}'\boldsymbol{R}\boldsymbol{T}(\alpha_\mathrm{f})\boldsymbol{R}^{-1}. \tag{28}$$

If we consider a stack of $2n$ layers symmetrical with respect to the midplane $X_3 = 0$, the stiffness matrix associated with this composite is,

$$\boldsymbol{D}_\mathrm{comp} = \sum_{k=1}^{n} \frac{2}{3}(h_k^3 - h_{k-1}^3)\bar{\boldsymbol{C}}_k(\alpha_{\mathrm{f}k}). \tag{29}$$

h_k refers to the X_3 (thickness) coordinate of the interface between layer k and layer $k-1$. $h_k \in [0, h_\mathrm{cloak}/2]$ for $k = \{0, 1, ..., n\}$. Each layer is made of a given UD material $\bar{\boldsymbol{C}}_k$ with a given fiber orientation $\alpha_{\mathrm{f}k}$.

4.2 Optimization problem

Now that the stiffness matrix coefficients of a laminated composite have been defined, based on the mechanical properties of a real input material, we formulate here the design as an optimization problem. Considering an isotropic host material with a certain thickness h_host, it is possible to compute $\boldsymbol{D}_\mathrm{iso}$ from equation (8), and then the stiffness tensor $\boldsymbol{D}$ for cloaking layers using (17). θ is here set to $\pi/6$ rad. We then seek the composite laminate that minimizes the cumulative relative error λ:

$$\lambda = \sum_{ij} \left| \frac{(D_\mathrm{comp})_{ij} - D_{ij}}{D_{ij}} \right| + \left| \frac{\rho_\mathrm{comp} - \rho}{\rho} \right|, \tag{30}$$
$$ij = \{11, 12, 16, 26, 66\}.$$

We also set several optimization constraints related to the manufacturing process:

- Cloaking layers' thicknesses must be the same as the host plate ($h_\mathrm{cloak} = h_\mathrm{host}$).
- Angles of fibers within the different layers of the laminate are equals ($\alpha_{\mathrm{f}k} = \alpha_\mathrm{f}$).

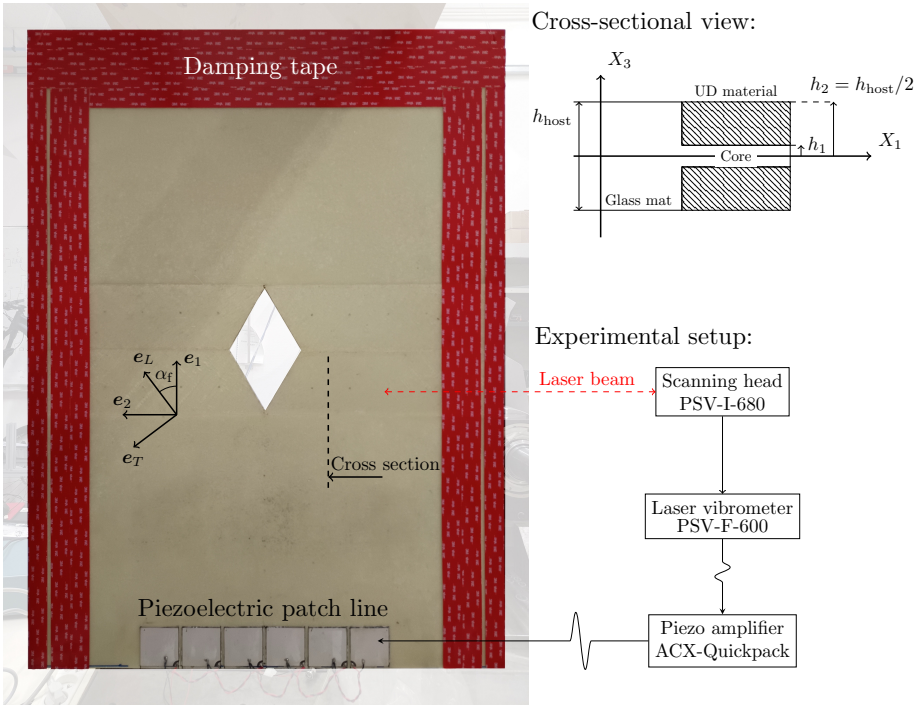

Figure 7: Photo of the experimental setup with the manufactured cloak and cross-sectional view of the layer assembly in the (X_1, X_3) plane.

- UD materials used within the different layers of the laminate are the same ($\bar{\boldsymbol{C}}_k = \bar{\boldsymbol{C}}$).
- The host plate and the laminated cloak composite are assembled using a core, an extension of the central part of the host plate that serves as a support for the assembly of the structure (see the cross-section representation in Figure 7).

Taking into account the dispersion analysis of the theoretical cloak, and noting that the fiber orientation angle is given by the highest phase velocity $v_\mathrm{p} = \omega/k$ [48], we set $\alpha_\mathrm{f}^{(1,3)} = -\alpha_1^{(1,3)}$ and $\alpha_\mathrm{f}^{(2,4)} = -\alpha_2^{(2,4)}$. Taking a pair of compatible materials, the only optimization variable is the degree of freedom $\beta(\theta = \pi/6)$ in (17). We then perform several optimizations using Matlab's genetic algorithm with different pairs of materials. This allows to evaluate how closely a given assembly, approximates the set of theoretical solutions in (17). The optimal configuration appears to be a glass mat host plate and an UD glass fiber material for the cloak. Elasticity matrix in GPa of glass mat is given in global basis $(\boldsymbol{e}_1, \boldsymbol{e}_2)$:

$$\boldsymbol{C}_\mathrm{mat} = \begin{pmatrix} 19.832 & 6.570 & 2.067 & 0 & 0 & 0 \\ & 19.832 & 2.067 & 0 & 0 & 0 \\ & & 4.824 & 0 & 0 & 0 \\ & & & 6.631 & 0 & 0 \\ & & & & 6.631 & 0 \\ & \text{Sym.} & & & & 6.631 \end{pmatrix}. \tag{31}$$

Elasticity matrix in GPa of UD material is given in the local basis $(\boldsymbol{e}_L, \boldsymbol{e}_T)$:

$$\boldsymbol{C}'_\mathrm{UD} = \begin{pmatrix} 52.745 & 5.926 & 5.926 & 0 & 0 & 0 \\ & 12.752 & 4.677 & 0 & 0 & 0 \\ & & 12.752 & 0 & 0 & 0 \\ & & & 4.037 & 0 & 0 \\ & & & & 4.033 & 0 \\ & \text{Sym.} & & & & 4.033 \end{pmatrix}. \tag{32}$$

The cloak shown (visible in Figure 7) was manufactured using vacuum (-0.5 bar) infusion process [54] at room temperature (20°C). Polymerization time is 24 hours for Polyprocess SPI 725 ACC45 polyester resin. The thickness dimensions are $h_1 = 0.27$ mm and $h_2 = 1.68$ mm and the plate is 835 mm long and 625 mm wide.

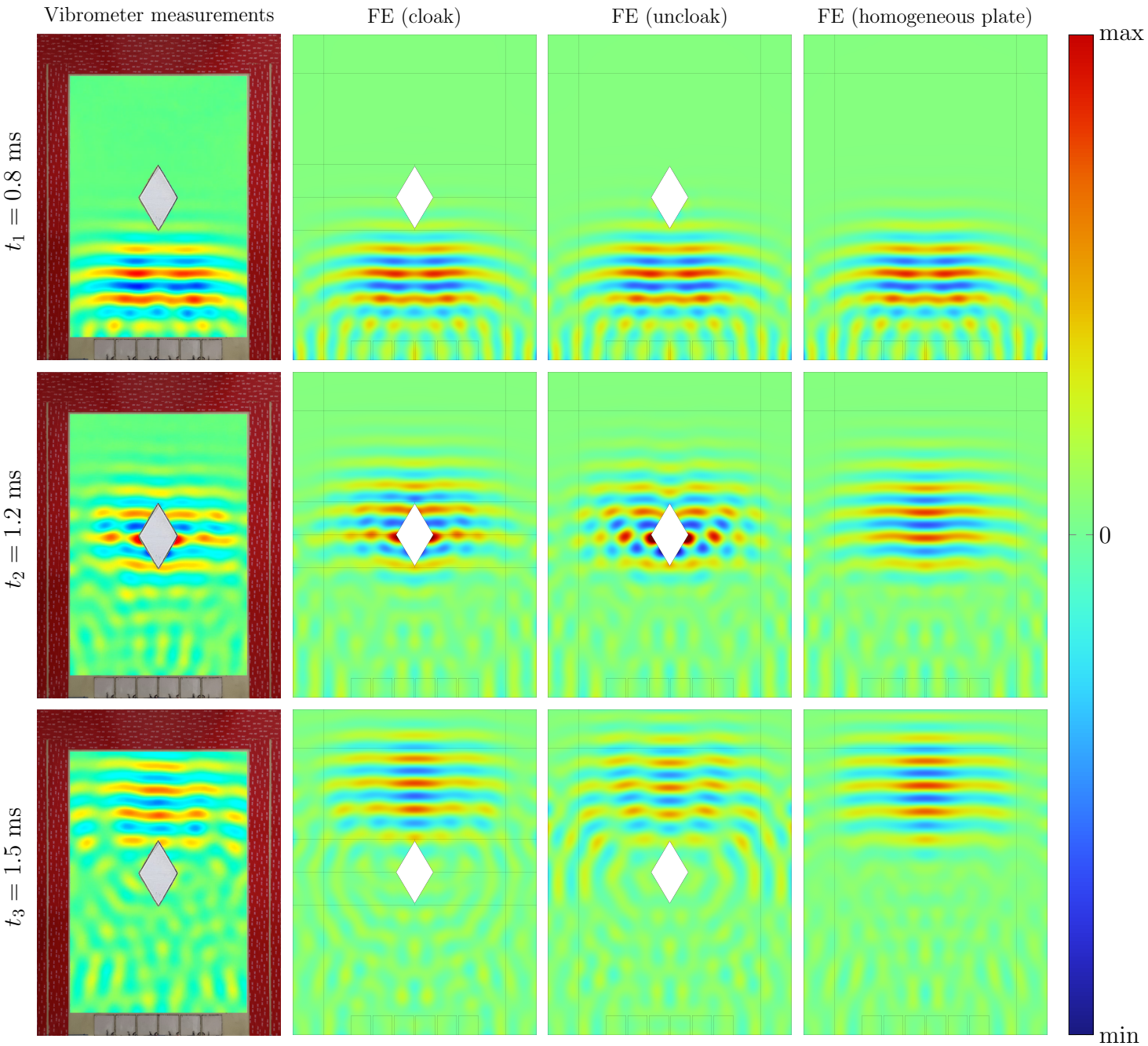

Figure 8: Comparison between experimentally measured out-of-plane velocity [m/s] and FE-computed out-of-plane velocity. The burst is the same as in numerical simulations with parameters refered in Table 1.

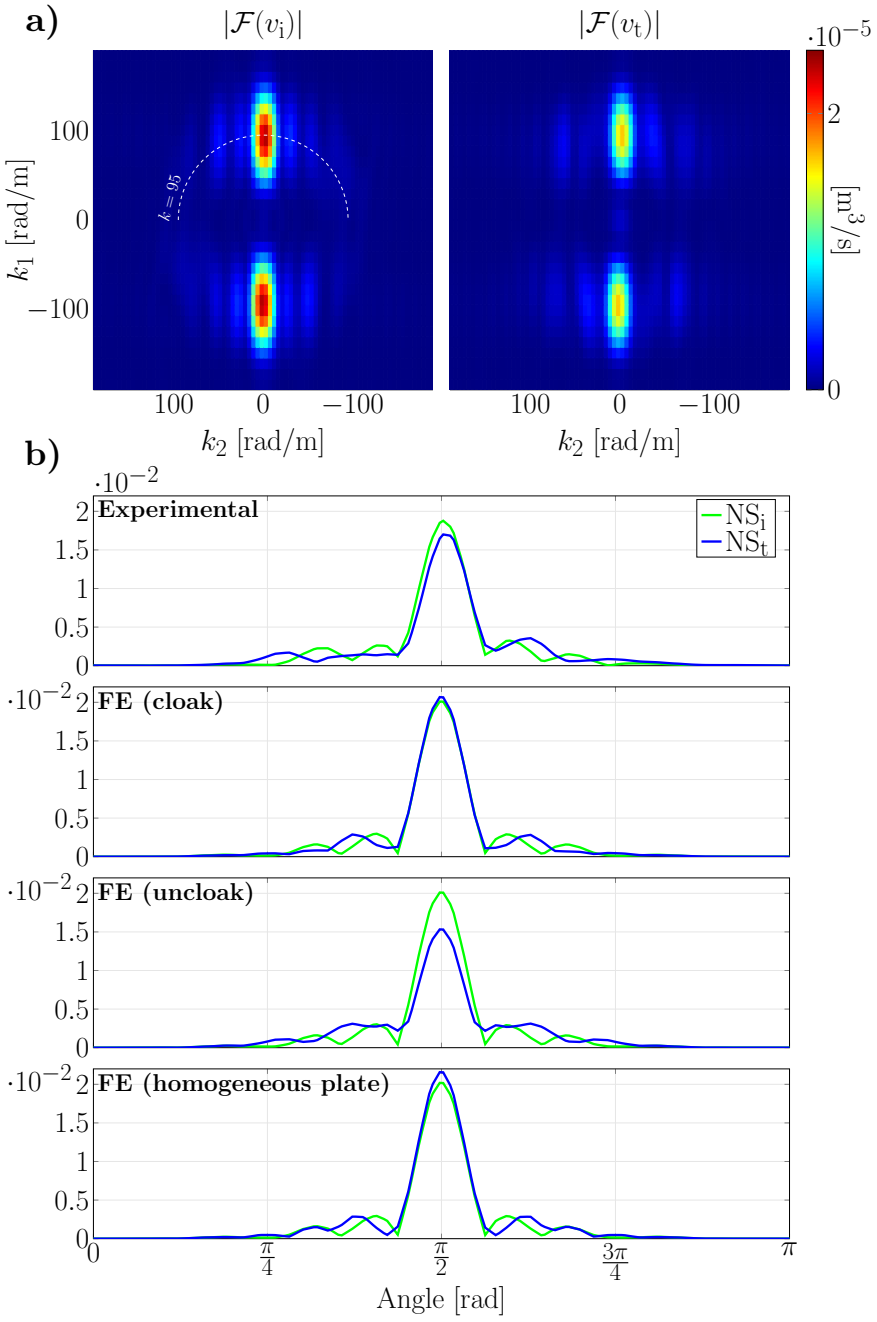

Figure 9: **a)** Spectra of incident out-of-plane velocity v_i and transmitted velocity v_t of experimental measurements. **b)** Normalized Spectra (NS) for wavenumber isovalues $k = 95$ rad/m, for experimental measurements, FE-computed cloak, uncloaked hole and homogeneous plate.

5 Experimental validation

In order to validate the proposed design methodology, we are now performing temporal measurements using a Polytech PSV-F-600 laser vibrometer with a PSV-I-680 sensor head. The burst already used in the numerical simulations with parameters refered in Table 1, is generated by an array of $50 \times 50 \times 1$ mm Ferroperm PZ26 piezoelectric patches glued along bottom edge of the host plate. Piezoelectric patches are polarized in the out-of-plane direction with a piezoelectric coupling coefficient $d_{31} = -1.3.10^{-10}$ C/N. We use an ACX Quick-pack piezo amplifier to increase voltage to 4.5 V. The amplifier's gain is 5.35 V/V. 3M VHB 4910 damping tape is affixed to the edges of the plate in order to limit the influence of the free edges on the wave field and to take cleaner measurements (see the suspended plate in Figure 7). In addition to experimental measures, numerical experiments modeling the manufactured plate equipped with the piezoelectric patches is performed in COMSOL Multiphysics using the solid mechanics/piezoelectricity coupling module. The burst is specified as a voltage Dirichlet boundary condition with an amplitude of 4.5 V on all the piezoelectric patches' electrodes. Dissipation caused by the damping tape is modeled using a Rayleigh law with an stiffness damping parameter of 5.3 µs. We also provide the finite element simulation of the uncloaked hole and the homogeneous plate as a reference. A comparison of the out-of-plane velocity field [m/s] experimentally measured by the vibrometer and the corresponding numerical experiments is presented in Figure 8. Firstly, we see a good match between vibrometer measurements and the associated numerical experiment. This shows that the elasticity matrices (31) and (32) accurately model the elasticity of the actual structure. Secondly, we note that in the numerical case, the cloak seems to effectively reconstructs the plane wave with minimal distortion and back reflection of the wavefront. Although these trends are also observed in experimental case, measurements show that the manufactured cloak tends to distort the wavefront more significantly due to manufacturing imperfections in the assembly of composite materials and piezoelectric array. The suppression of scattering upstream of the manufactured cloak is likely aided by the inherent damping of composite materials. However, in the associated numerical simulation, damping other than that of the lateral layers is not modeled, and the reflected component appears to be minimal. Thirdly, we note that the uncloaked hole causes more back reflection and tends to scatter the wave laterally. The transmitted wavefront appears more disturbed compared to those passing through the cloak or the reference plane wave.

In order to better investigate the experimental measurements, we analyse the spatial spectra (k-space representation) associated with times $t = t_1$ (incident out-of-plane velocity wave v_i) and $t = t_3$ (transmitted out-of-plane velocity wave v_t). This has been done using 2-Dimensional Fast Fourier Transform (2D FFT). 2D FFT modules are given in Figure 9 **a)**. The spectrum of v_i is mainly concentrated along the k_1-direction (plane wave), and the size of the lobe along this direction reveals the broad frequency content. Additional lateral lobes of low amplitude appear due to the spherical components of the excitation as well as

residual reflections in absorbing layers. The spectrum of v_t is slightly disturbed laterally, which reveals the scattered component generating the planeness defect visible in Figure 8. In addition, the amplitude of the transmitted spectrum peak tends to decrease due to damping.
To quantify cloaking quality, we use the Normalized Spectrum (NS) of incident wave, $\mathrm{NS_i} = |\mathcal{F}(v_i)| / \int_{k_1>0} |\mathcal{F}(v_i)| \mathrm{d}k_1 \mathrm{d}k_2$ and transmitted wave $\mathrm{NS_t} = |\mathcal{F}(v_t)| / \int_{k_1>0} |\mathcal{F}(v_t)| \mathrm{d}k_1 \mathrm{d}k_2$. Normalization by integration over the domain of interest for $k_1 > 0$ allows the cloaking deficiency to be quantified independently of composite's damping. The normalized spectra are plotted in figure 9 **b)** for the wavenumber isovalues $k = 95$ rad/m, passing through the peak of the spectra. This is performed for experimental measurements as well as FE simulation of the cloak, the uncloaked hole and the reference homogeneous plate. The normalized transmitted spectrum for the experimental measurements is asymmetric due to manufacturing defects. However, the planar incident component around $\pi/2$ rad is correctly reconstructed. The relative error between the maxima of the incident and transmitted normalized spectra is $(\mathrm{NS_t} - \mathrm{NS_i})/\mathrm{NS_i} = -9.6\%$. The normalized spectra obtained from simulations of the cloak, in which these defects do not appear, yield better results. Around $\pi/2$ rad, the two curves merge, and the relative error between the maxima is 3%. This is also true for simulations of the homogeneous host plate. The relative error of the maxima is, however, slightly higher (7%) than the one of the cloak simulations because the incident spherical components tend to focus at the center of the plate. This is clearly visible in the figure 8. In the case of the cloak simulations, these components are likely reflected backward by the hole and are therefore less visible in the transmitted spectrum. In the case of the uncloaked hole, the normalized transmitted spectrum is drastically disrupted. The relative error of the maxima increases to -24%, and a larger portion of the transmitted wave is scattered in lateral directions. Despite its manufacturing imperfections, the cloaking device is therefore capable of reproducing the intended effect as predicted by numerical simulations.

6 Conclusion & perspectives

In this article, we demonstrate the feasibility of broadband flexural cloaking. By reducing the general problem of omnidirectional cloaking in plates to an unidirectional case, we theoretically and numerically demonstrate the existence of a purely anisotropic cloak. An analysis of the cloak's dispersion reveals the phase and group velocity fields required to achieve such a phenomenon. We then present a design methodology based on the optimization of a real composite material to best approximate the theoretically determined constitutive laws. The resulting manufactured cloak is tested experimentally using vibrometer measurements. Good agreement between experimental measurements and the FE-computed plane wave solution is observed. A detailed analysis of the spectra of incident and transmitted waves reveals that, despite manufacturing imperfections, the fabricated cloak tends to reproduce the cloaking performance

observed in the simulations. This device has the advantage of being easily manufactured using well-known manufacturing techniques. Contrary to most of the proposition of the literature, no heterogeneous constitutive laws are required, as well as additional terms of lower order in the propagation equation. In addition, the constant thickness and simple layering make it easy to fabricate and control manufacturing uncertainties. However, while this proof of concept confirms the validity of the design method, further efforts are required to increase cloaking efficiency. For example, a more complex laminate could provide a better approximation of the theoretical solution. Additionally, better accounting for the composite's damping in the simulations would be useful for improving the accuracy of the models. We believe that this preliminary work will pave the way for generalization to the omnidirectional case, as well as other bending wave phenomena based on transformation method (black hole effect, mirages, *etc.*). The angle of incidence robustness analysis for the theoretical model shows that cloaking quality remains acceptable for small misalignments. Then, omnidirectionality could be achieved by designing a cloak whose geometry possesses more central rotational symmetries. See Supplemental Material for videos of time simulations and acquisitions (figures 3 and 8).

7 Acknowledgments

The authors would like to thank l'Agence Nationale de la Recherche (ANR) for funding the ASTRIA research project under the grant number ANR-21-CE46-001-05.

References

[1] J. B. Pendry, D. Schurig, and D. R. Smith, "Controlling Electromagnetic Fields," *Science*, vol. 312, pp. 1780–1782, June 2006.

[2] U. Leonhardt, "Optical Conformal Mapping," *Science*, vol. 312, no. 5781, pp. 1777–1780, 2006.

[3] D. Schurig, J. J. Mock, B. J. Justice, S. A. Cummer, J. B. Pendry, A. F. Starr, and D. R. Smith, "Metamaterial Electromagnetic Cloak at Microwave Frequencies," *Science*, vol. 314, no. 5801, pp. 977–980, 2006.

[4] W. Cai, U. K. Chettiar, A. V. Kildishev, and V. M. Shalaev, "Optical cloaking with metamaterials," *Nature Photonics*, vol. 1, pp. 224–227, Apr. 2007.

[5] S. Zhang, C. Xia, and N. Fang, "Broadband Acoustic Cloak for Ultrasound Waves," *Physical Review Letters*, vol. 106, p. 024301, Jan. 2011.

[6] D. J. Colquitt, I. S. Jones, N. V. Movchan, A. B. Movchan, M. Brun, and R. C. McPhedran, "Making waves round a structured cloak: lattices, negative refraction and fringes," *Proceedings of the Royal Society A: Mathematical, Physical and Engineering Sciences*, vol. 469, p. 20130218, Sept. 2013.

[7] M. Kadic, T. Bückmann, R. Schittny, and M. Wegener, "Experiments on cloaking in optics, thermodynamics and mechanics," *Philosophical Transactions of the Royal Society A: Mathematical, Physical and Engineering Sciences*, vol. 373, p. 20140357, Aug. 2015.

[8] A. Zareei and M.-R. Alam, "Cloaking in shallow-water waves via nonlinear medium transformation," *Journal of Fluid Mechanics*, vol. 778, pp. 273–287, 2015. Edition: 2015/07/30.

[9] Y. Chen, M. Zheng, X. Liu, Y. Bi, Z. Sun, P. Xiang, J. Yang, and G. Hu, "Broadband solid cloak for underwater acoustics," *Physical Review B*, vol. 95, p. 180104, May 2017.

[10] M. Cassier, T. DeGiovanni, S. Guenneau, and F. Guevara Vasquez, "Active thermal cloaking and mimicking," *Proceedings of the Royal Society A: Mathematical, Physical and Engineering Sciences*, vol. 477, no. 2249, p. 20200941, 2021.

[11] A. N. Norris, "Acoustic metafluids," *The Journal of the Acoustical Society of America*, vol. 125, pp. 839–849, Feb. 2009.

[12] A. N. Norris, "Acoustic cloaking theory," *Proceedings of the Royal Society A: Mathematical, Physical and Engineering Sciences*, vol. 464, pp. 2411–2434, Sept. 2008.

[13] A. N. Norris, "Acoustic cloaking in 2D and 3D using finite mass," Feb. 2008. arXiv:0802.0701 [physics].

[14] Y. Chen, X. Liu, and G. Hu, "Latticed pentamode acoustic cloak," *Scientific Reports*, vol. 5, p. 15745, Oct. 2015.

[15] G. W. Milton, M. Briane, and J. R. Willis, "On cloaking for elasticity and physical equations with a transformation invariant form," *New Journal of Physics*, vol. 8, pp. 248–248, Oct. 2006.

[16] M. Brun, S. Guenneau, and A. B. Movchan, "Achieving control of in-plane elastic waves," *Applied Physics Letters*, vol. 94, p. 061903, Feb. 2009.

[17] A. Norris and A. Shuvalov, "Elastic cloaking theory," *Wave Motion*, vol. 48, pp. 525–538, Sept. 2011.

[18] Y. Achaoui, A. Diatta, M. Kadic, and S. Guenneau, "Cloaking In-Plane Elastic Waves with Swiss Rolls," *Materials*, vol. 13, p. 449, Jan. 2020.

[19] H. Zhang, Y. Chen, X. Liu, and G. Hu, "An asymmetric elastic metamaterial model for elastic wave cloaking," *Journal of the Mechanics and Physics of Solids*, vol. 135, p. 103796, Feb. 2020.

[20] M. Farhat, S. Guenneau, S. Enoch, and A. B. Movchan, "Cloaking bending waves propagating in thin elastic plates," *Physical Review B*, vol. 79, p. 033102, Jan. 2009.

[21] M. Farhat, S. Guenneau, and S. Enoch, "Ultrabroadband Elastic Cloaking in Thin Plates," *Physical Review Letters*, vol. 103, p. 024301, July 2009.

[22] M. Farhat, S. Guenneau, and S. Enoch, "Broadband cloaking of bending waves via homogenization of multiply perforated radially symmetric and isotropic thin elastic plates," *Physical Review B*, vol. 85, p. 020301, Jan. 2012.

[23] A. Climente, D. Torrent, and J. Sánchez-Dehesa, "Analysis of flexural wave cloaks," *AIP Advances*, vol. 6, p. 121704, Dec. 2016.

[24] A. Golgoon and A. Yavari, "Transformation Cloaking in Elastic Plates," *Journal of Nonlinear Science*, vol. 31, p. 17, Feb. 2021.

[25] N. Stenger, M. Wilhelm, and M. Wegener, "Experiments on Elastic Cloaking in Thin Plates," *Physical Review Letters*, vol. 108, p. 014301, Jan. 2012.

[26] D. Misseroni, D. J. Colquitt, A. B. Movchan, N. V. Movchan, and I. S. Jones, "Cymatics for the cloaking of flexural vibrations in a structured plate," *Scientific Reports*, vol. 6, p. 23929, Apr. 2016.

[27] D. Colquitt, M. Brun, M. Gei, A. Movchan, N. Movchan, and I. Jones, "Transformation elastodynamics and cloaking for flexural waves," *Journal of the Mechanics and Physics of Solids*, vol. 72, pp. 131–143, Dec. 2014.

[28] M. Brun, D. J. Colquitt, I. S. Jones, A. B. Movchan, and N. V. Movchan, "Transformation cloaking and radial approximations for flexural waves in elastic plates," *New Journal of Physics*, vol. 16, p. 093020, Sept. 2014.

[29] S. Timoshenko and S. Woinowsky-Krieger, *Theory of Plates and Shells*. Engineering mechanics series, McGraw-Hill, 1959.

[30] S. Lekhnitskii, *Anisotropic Plates*. Clearinghouse for Federal Scientific & Technical Information, 1967.

[31] L. Pomot, S. Bourgeois, C. Payan, M. Remillieux, and S. Guenneau, "On form invariance of the Kirchhoff-Love plate equation," Dec. 2018. arXiv:1901.00067 [physics].

[32] K. Tang, C. Xu, S. Guenneau, and P. Sebbah, "Pulse dynamics of flexural waves in transformed plates," Feb. 2021. arXiv:2008.12402 [physics].

[33] K. Tang, E. Luz, D. Amram, L. Kadysz, S. Guenneau, and P. Sebbah, "Dynamic cloaking of a diamond-shaped hole in elastic plate," *Applied Physics Letters*, vol. 122, p. 011701, Jan. 2023.

[34] K. Tang, C. Xu, E. Luz, D. Amram, L. Kadysz, J. Wang, S. Guenneau, and P. Sebbah, "Tailoring transient flexural-wave propagation in transformed plates," *Journal of Applied Physics*, vol. 139, Mar. 2026.

[35] D. Misseroni, A. B. Movchan, and D. Bigoni, "Omnidirectional flexural invisibility of multiple interacting voids in vibrating elastic plates," *Proceedings of the Royal Society A: Mathematical, Physical and Engineering Sciences*, vol. 475, p. 20190283, Sept. 2019.

[36] F. Legrand, B. Gérardin, F. Bruno, J. Laurent, F. Lemoult, C. Prada, and A. Aubry, "Cloaking, trapping and superlensing of lamb waves with negative refraction," *Scientific Reports*, vol. 11, p. 23901, Dec. 2021.

[37] G. W. Milton, ed., *The Theory of Composites*. Salt Lake City, Utah: Milton & Patton Publishing, 2016.

[38] J. C. Gerdeen and R. A. L. Rorrer, *Engineering Design with Polymers and Composites, Second Edition*. Dec. 2011.

[39] M. A. Neto, A. Amaro, L. Roseiro, J. Cirne, and R. Leal, "Finite Element Method for Plates/Shells," in *Engineering Computation of Structures: The Finite Element Method*, pp. 195–232, Cham: Springer International Publishing, 2015.

[40] P. Garambois, S. Besset, and L. Jézéquel, "Various double component mode synthesis and sub-structuring methods for dynamic mixed FEM," *European Journal of Mechanics - A/Solids*, vol. 53, pp. 196–219, Sept. 2015.

[41] L. Chen, J. Hu, and X. Huang, "Multigrid Methods for Hellan–Herrmann–Johnson Mixed Method of Kirchhoff Plate Bending Problems," *Journal of Scientific Computing*, vol. 76, pp. 673–696, Aug. 2018.

[42] K. Rafetseder, *A New Approach to Mixed Methods for Kirchhoff-Love Plates and Shells*. PhD thesis, Johannes Kepler Universität, Linz, 2018.

[43] D. N. Arnold and S. W. Walker, "The Hellan-Herrmann-Johnson method with curved elements," July 2020. arXiv:1909.09687 [math].

[44] D. O'Boy, V. Krylov, and V. Kralovic, "Damping of flexural vibrations in rectangular plates using the acoustic black hole effect," *Journal of Sound and Vibration*, vol. 329, pp. 4672–4688, Oct. 2010.

[45] A. Pelat, F. Gautier, S. C. Conlon, and F. Semperlotti, "The acoustic black hole: A review of theory and applications," *Journal of Sound and Vibration*, vol. 476, p. 115316, June 2020.

[46] K. Graff, *Wave Motion in Elastic Solids*. Oxford engineering science series, Ohio State University Press, 1975.

[47] D. A. Kiefer, S. Mezil, and C. Prada, "Beating resonance patterns and extreme power flux skewing in anisotropic elastic plates," *Science Advances*, vol. 9, p. eadk6846, Dec. 2023.

[48] F. Hervin and P. Fromme, "Guided wave propagation and skew effects in anisotropic carbon fiber reinforced laminates," *The Journal of the Acoustical Society of America*, vol. 153, pp. 2049–2060, Apr. 2023.

[49] D. A. Kiefer, S. Mezil, and C. Prada, "Extreme wave skewing and dispersion spectra of anisotropic elastic plates," *Physical Review Research*, vol. 7, p. L012043, Feb. 2025.

[50] J. Berthelot and J. Cole, *Composite Materials: Mechanical Behavior and Structural Analysis*. Mechanical Engineering Series, Springer New York, 1999.

[51] J. Zhao, B. Bonello, and O. Boyko, "Focusing of the lowest-order antisymmetric Lamb mode behind a gradient-index acoustic metalens with local resonators," *Physical Review B*, vol. 93, p. 174306, May 2016.

[52] G. J. Chaplain and R. V. Craster, "Flat lensing by graded line metaarrays," *Physical Review B*, vol. 99, p. 220102, June 2019.

[53] V. Rapine, N. Abuhemeida, M. Ouisse, S. Cogan, P. Francescato, R. Lachat, and Y. Meyer, "A composite gradient index lens for wideband elastic waves focusing: Design approach and experimental validation at constant thickness," *Composite Structures*, vol. 372, p. 119500, Nov. 2025.

[54] J. Summerscales and T. J. Searle, "Low-pressure (vacuum infusion) techniques for moulding large composite structures," *Proceedings of the Institution of Mechanical Engineers, Part L: Journal of Materials: Design and Applications*, vol. 219, pp. 45–58, Jan. 2005.